NMR structure of duplex DNA containing the Î±-OH-PdGâ¢dA base pair: A mutagenic intermediate of acrolein

ARTICLE *in* BIOPOLYMERS · JANUARY 2009

Impact Factor: 2.39 · DOI: 10.1002/bip.21366 · Source: PubMed

6 AUTHORS, INCLUDING:

Tanya Zaliznyak
Stony Brook University
9 PUBLICATIONS **168** CITATIONS
SEE PROFILE

Mark Lukin
Stony Brook University
14 PUBLICATIONS **220** CITATIONS
SEE PROFILE

Francis Johnson
Stony Brook University
252 PUBLICATIONS **6,976** CITATIONS
SEE PROFILE

Published in final edited form as:
Biopolymers. 2010 April ; 93(4): 391–401. doi:10.1002/bip.21366.

NMR Structure of Duplex DNA Containing the α-OH-PdG•dA Base Pair: a Mutagenic Intermediate of Acrolein

Tanya Zaliznyak, **Mark Lukin**, **Mahmoud El-khateeb**[†], **Rahda Bonala**, **Francis Johnson**, and **Carlos de los Santos**[*]
Department of Pharmacological Sciences, Stony Brook University, School of Medicine Stony Brook, New York 11794-8651

Abstract

Acrolein, a cell metabolic product and main component of cigarette smoke, reacts with DNA generating α-OH-PdG lesions, which have the ability to pair with dATP during replication thereby causing G to T transversions. We describe the solution structure of an 11-mer DNA duplex containing the mutagenic α-OH-PdG•dA base pair intermediate, as determined by solution NMR spectroscopy and retrained molecular dynamics simulations. The NMR data support a mostly regular right-handed helix that is only perturbed at its center by the presence of the lesion. Undamaged residues of the duplex are in *anti* orientation, forming standard Watson-Crick base pairs alignments. Duplication of proton signals at and near the damaged base pair reveals the presence of two enantiomeric duplexes, thus establishing the exocyclic nature of the lesion. The α-OH-PdG adduct assumes a *syn* conformation pairing to its partner dA base that is protonated at pH 6.6. The three-dimensional structure obtained by restrained molecular dynamics simulations show hydrogen bond interactions that stabilize α-OH-PdG in a *syn* conformation and across the lesion containing base pair. We discuss the implications of the structures for the mutagenic bypass of acrolein lesions.

INTRODUCTION

The simplest α,β-unsaturated aldehyde, propenal or acrolein, is widespread in the environment (1). The chemical industry produces ton amounts of acrolein each year as a starting material for the synthesis of polymers and simple organic substances. The incomplete combustion of organic materials, such as wood, fuel, food and tobacco are further sources of acrolein in the environment. Depending on the type of tobacco and its commercial brand, cigarette smoke has between 18–98 μg of acrolein per cigarette, quantities that far surpass the nanograms amounts of polycyclic aromatic hydrocarbons (PAH) or nitrosamines (2). Expectedly, lung tissues of smokers contain higher levels of acrolein-derived adducts than those generated by PAH (3). In addition to its environmental sources, lipid peroxidation (4–6) and polyamines metabolism (7) generate significant amounts of acrolein that damage cellular DNA. Moreover, lymphocytes of patients treated with cyclophosphamide, whose cell metabolism produces acrolein, contain significant amounts of acrolein-derived DNA adducts (8,9).

Acrolein reacts with DNA and proteins via Michael addition without requiring metabolic activation (10–12). In double-stranded DNA, acrolein produces two isomeric adducts, the major γ-OH-PdG product, after Michael addition to the peripheral amino group of dG, and the minor α-OH-PdG (Figure 1) adduct, that results from initial attack to the N1 position

[*]Corresponding author: cds@pharm.stonybrook.edu, phone: (631) 444-3649, fax (631) 444-3218.
[†]Present address Boehringer-Ingelheim Roxane Inc., Columbus OH, 43215

(11). Both lesions disrupt the ability of dG to form Watson-Crick (WC) hydrogen bonds and, thus, should exhibit genotoxic effects. Early studies using acrolein-treated prokaryotic or eukaryotic cells detected frequent base substitution mutations, primarily G•C → T•A transversions and G•C → A•T transitions (13–16). However, adduct-specific studies were not possible at that time. Following progress in DNA synthesis that has made possible the preparation of site- and lesion-specific oligomers (17–20), the mutagenic properties of each adduct has been reevaluated (21–24). Unexpectedly, DNA replication across γ-OH-PdG lesions is efficient and mostly (>99%) accurate in both bacterial and mammalian cells (21–23). On the other hand, α-OH-PdG significantly blocks DNA replication in human cells and, when bypassed by TLS polymerases, promotes the incorporation of dC along with G → T and G → A substitution mutations (24).

Simultaneously with these studies, we reported the NMR characterization of an 11-mer duplex having a γ-OH-PdG•dC pair at its center showing that the adduct adopts a ring open conformation and forms canonical WC hydrogen bonds with dC, providing a molecular mechanism that supports the accurate DNA replication across the lesion (25). More recently, we have described the solution structure of a cognate duplex having a α-OH-PdG•dC base pair, establishing that the acrolein lesion remains in the ring close form, assumes a *syn* conformation at its glycosidic angle and is hydrogen bonded to the counter cytosine residue, which is protonated at pH 5.9 (26). Outside the lesion site adjustments, the duplex mostly adopts a regular right-handed helical conformation with Watson-Crick hydrogen bonds stabilizing all undamaged base pairs of the duplex. To understand further the molecular mechanisms of acrolein toxicity, this study describes the solution structure of a related duplex that contains the mutagenic α-OH-PdG•dA base pair at its center (hereinafter called the α-OH-PdG•dA duplex). The companion manuscript (Minetti et al., 2009) (41) reports the impact of α-OH-PdG on the thermal and thermodynamic stability of damaged duplexes and its overall opposite base-dependence. Figure 1 shows the chemical structure of acrolein-derived lesions and the duplex sequence employed in our study.

MATERIALS AND METHODS

Synthesis and purification of the oligomeric duplex

We prepared the damaged and undamaged oligodeoxynucleotides using standard solid phase synthesis methods, generating the α-OH-PdG adduct post-synthetically following published procedures (20). Briefly, we synthesized the 5'-*O*-dimethoxytrityl-3'-*O*-(β-cyanoethyl)-phosphoramidite derivative of 1-(3,4-diacetylbutyl)-N^2-(dimethylaminomethylene)-dG and used it to incorporate 1-(3,4-diacetoxybutyl)-dG at the center of the undecanucleotide. We purified the lesion-containing oligomer by HPLC, using a reverse-phase Luna 5 μm Phenyl-Hexyl (250×10 mm) column (Phenomenex, Torrance, CA). An initial run on dimethoxytritylated samples used a mobile phase consisting of a 16–36% acetonitrile gradient, over 35 min, in 0.1 M triethylammonium acetate (TEAA) buffer, pH 6.8. A second run followed the removal of the 5'-*O*-DMT group by reaction with 80% acetic acid for 30 minutes and used a 0–20% TEAA-acetonitrile gradient over 40 minutes. Room temperature treatment of the 1-(3,4-dihydroxybutyl)-dG containing oligomer with a 100 mM sodium periodate solution (0.5 M sodium acetate buffer, pH 6.0) for five minutes oxidatively cleaved the dihydroxy chain generating α-OH-PdG. A final HPLC purification of the oxidation reaction products yielded a single peak that corresponded to the desired oligomer. ESI-MS analysis revealed an m/z = 3373.9 ± 1.3 (theoretical mass 3373.2), verifying the identity of the lesion-containing strand. We purified the complementary unmodified oligonucleotide following similar procedures.

Duplex formation and sample preparation

We obtained the proper 1:1 strand ratio by following the intensity of selected NMR proton signals during the gradual addition of the unmodified to the lesion-containing oligomer. NMR samples consisted of 240 OD_{260} of duplex dissolved in 0.6 ml of 25 mM phosphate buffer, pH 6.6, containing 50 mM NaCl and 0.5 mM EDTA in either 99.96% D_2O (D_2O buffer) or 90% H_2O-10% D_2O (v/v) (H_2O buffer), corresponding to around 3.3 mM duplex concentration.

NMR experiments

We recorded NMR spectra on a Varian Inova spectrometer operating at 14.1 T. Proton chemical shifts were referenced relative to sodium 3-(trimethylsilyl)propionate-2,2,3,3-d_4 at 0 ppm. The NMR data set consisted of 1D proton spectra recorded in D_2O and H_2O buffer, 2D phase-sensitive (27) NOESY (90, 150, 200, and 300 ms mixing time), COSY, DQF-COSY and TOCSY (70 and 120 ms contact time) spectra in D_2O buffer at 25°C. A soft pre-saturation pulse at the water frequency suppressed the residual water signal present on D_2O experiments. We collected phase-sensitive proton NOESY spectra (120 and 220 ms mixing time) in H_2O buffer at 5°C using a 'jump-return' reading pulse (28). We processed the NMR data with Felix (Accelrys Inc., San Diego, CA) running operating on Silicon Graphics workstations. Typical 2D data sets consisted of 2048 by 300 complex points in the t_2 and t_1 dimensions, respectively. Prior to Fourier transformation, we filtered the time domain data by multiplication with shifted sine-bell window functions. We applied no baseline correction, or other 'data massaging' methods, to the frequency domain spectra.

Determination of the duplex structure

A refined structural model of the duplex was obtained employing restrained molecular dynamics (rMD) simulations with X-PLOR 3.1 (29). We used an all-atom force field derived from CHARMM (30) and the dielectric constant set to 4 (31). Charges of phosphate groups were unscreened, resulting in deoxynucleotide residues with a net −1 charge. The topology and partial charges of the lesion OH-propano ring were determined by analogy to the deoxyribose C_2H_2 (for β-CH_2 and γ-CH_2 groups) and C_1-O_4 (for α-CHOH). Computation of inter-proton distances followed the same full relaxation matrix approach recently described for the α-OH-PdG•dC duplex (26). Briefly, we used 1,000 steps of energy minimization, using a sole potential energy function that is proportional to the difference between back-calculated and experimental NOE intensities (32), to optimize the position of hydrogens on canonical B-form duplexes having the *R* or *S* isomer of α-OH-PdG in *syn* conformation. A grid search revealed that 2.33 ns was the best isotropic correlation time (τ_c) for fitting the experimental NOE intensities to the initial B-form duplex and this value was set during computation of the inter-proton distances. Experimental distances were extracted from the last atom coordinates set of the minimization. We measured the experimental NOE intensities with Felix using all D_2O NOESY spectra. Since we assigned NOE cross peaks at the center of the duplex stereo specifically, we computed independent sets of inter-proton distances for the *S* and *R* α-OH-PdG•dA duplexes (see results section). At the ends of the duplex, proton signals originating from each isomer are unresolved and, thus, each isomer assumed half of the peak intensities. This 50% split followed our previous observations with the α-OH-PdG•dC duplex (26). rMD simulations for the *R* isomer run implementing 548 distance restraints that were enforced using square-well potential energy functions, with boundaries of ±0.6 Å for non-overlapping cross-peaks and ±0.9 Å for those observed only in the 300 ms mixing time NOESY. Refinement of the *S* isomer proceeded with an identical number of distance restraints using the same values and boundary criteria. Following NMR data analysis, we run rMD enforcing W-C hydrogen bonds on all undamaged base pairs and backbone dihedral angles encompassing the B- and A-form conformation for the terminal four base pairs of the duplex.

The initial duplex structures had the *R* (or *S*) isomer of α-OH-PdG in *syn* conformation paired to a protonated adenosine residue. Prior to the rMD simulations, a short energy minimization relieved the unfavorable contacts present the initial models. The rMD protocols were identical to those recently implemented for the refinement of α-OH-PdG•dC duplexes (26). Briefly, we started rMD simulations from five different temperatures and heated the system to 500K on the first 100 ps. Inter-proton distance restraints were gradually enforced during the heating step with a penalty constant that increased from 10 to 300 kcal/(mol A^2) and remained at this value until the end of the simulation. Simulations run at high temperature for 100 to 120 ps, after which we slowly cooled down the system to 300K in 100 ps and equilibrated it by an additional 150 ps of rMD at this temperature. For each α-OH-PdG isomer we computed twenty five independent duplex structures by starting the simulations at different temperatures (100, 105, 110, 115, and 120K) and using five different time lengths of the high-temperature step (100, 105, 110, 115, and 120 ps). The last atom coordinates set of each run was energy-minimized generating an ensemble of distance-refined structures that converged with pair-wise Root Mean Square Deviations (RMSD) of <1.2 Å and <1.3 Å for the *S* and *R* isomers, respectively. Each ensemble was averaged and energy minimized, yielding the structure of isomeric α-OH-PdG•dA duplexes presented here. We refined 50 additional structures of the duplex, 25 for each isomer, using identical rMD protocols but with the lesion partner A17 in a non-protonated state. Structures were analyzed with Curves (33) and visualized with Chimera (34) or InsightII (Accelrys Inc., San Diego, CA).

RESULTS

Non-exchangeable proton spectra

The one-dimensional spectrum of the α-OH-PdG•dA duplex in 100% D_2O phosphate buffer at 25°C, shown in Figure 1S (Supplementary Information) displays reasonably sharp and well-resolved proton signals, indicating that the sample is amenable to NMR structure determination. The assignment of non-exchangeable protons of the duplex resulted from the analysis of NOESY, COSY and TOCSY spectra following established procedures (35, 36). Figure 2 shows an expanded region of the 300 ms mixing time NOESY spectrum illustrating the interactions between the base (6.96–8.45 ppm) and sugar-H1' (4.87–6.36 ppm) protons on the central part of the duplex. Each purine-H8 or pyrimidine-H6 proton on the undamaged strand shows cross peaks to the H1′ proton of the same and 5′-flanking residues (Figure 2, right panel), establishing a right-handed helical conformation for the duplex. NOE peaks clearly identify residues on the C1–C5 and C7–C11 stretches of the duplex (Figure 2, left panel), but interactions break at the damaged residue where the α-OH-PdG(H8)-C7(H1') cross peak substitutes the expected α-OH-PdG(H8)-C5(H1') interaction (Figure 2, peaks D). In addition, the α-OH-PdG(H8-H1') NOE cross peak is unusually strong (Figure 2, left panel, peak X6) a fact that establishes a short distance between these protons and suggests a *syn* conformation around the glycosidic bond of the adduct. The *syn* conformation of α-OH-PdG readily explains the loss of the sequential interaction with C5(H1') and the observation of an NOE interaction with C7(H1'). The interaction between the sugar-H1' and the adenine-H2 protons (Figure 2, peaks D–P) and between the purine-H8 and the 3'-attached cytosine-H5 protons (Figure 2, peaks Q–T) is further evidence of the right-handed conformation for the α-OH-PdG•dA duplex in solution. Figure 2S (Supplementary Information) presents the full 'NOE walk' on the damaged duplex.

A peculiar feature revealed by the NOESY spectrum shown in Figure 2, which was previously observed during our characterization of the α-OH-PdG•dC duplex (26), is the splitting of NMR signals at the center of the duplex. Such cross peak splitting is also present in other regions of the NOESY spectrum at 25°C (Figure 3) and in interactions observed among the exchangeable protons of the duplex at 5°C (Figure 4). This characteristic feature

originates from the presence of the chiral α-OH-PdG(Cα) atom (Figure 1) and affects protons located at the center of the duplex. Enantiomer specific assignments follows the observation of the α-OH-PdG(Hα)-C5(H6) cross peak (Figure 2, peak A), expected only in the case of the *S* isomer that orients its Hα proton towards the 5'-flanking residue after the adduct rotates to a *syn* conformation. For the complementary strand, the identification of two A20(H2)-A4(H1') cross peaks (Figure 2, peak N) lead to the isomer specific assignment of the A20(H2) protons, from here to that of A20(H1') (Figure 2, peak M) and, subsequently, of all other resolved cross peaks on the undamaged strand (Figure 2, right panel). Analysis of COSY and TOCSY spectra recorded under identical conditions confirmed these assignments.

Assignment of the exocyclic α-OH-PdG protons resulted from the examination of a different region of the same 300 ms mixing time NOESY spectrum (Figure 3). The α-OH-PdG(Hα) signal at 5.26 ppm, which exhibited an NOE cross peak to C5(H6) (Figure 2, peak A), shows strong and weak interactions with the β and γ protons of the (*S*) α-OH-PdG isomer (Figure 3, peaks B and A, respectively). Similarly, the α-OH-PdG(Hα) signal of the *R* isomer at 5.20 ppm displays strong NOE peaks with the β and γ protons (Figure 3, peaks D and C), completing the proton assignments of the α-OH-PdG adduct. In addition to these intra-residue interactions, protons of the OH-PdG ring show several NOE peaks with protons of the 5'-flanking residue (Figure 3, peaks F–I), which provide valuable distance restraints for refinement of the duplex solution structure. The chemical shift of non-exchangeable protons on the α-OH-PdG•dA duplex are listed in Table 1S (Supplementary Information).

Exchangeable proton spectra

A 600 MHz proton spectrum, recorded at 5°C in pH 6.6 phosphate buffer solution, displays eleven partially resolved signals in the 13.70–12.10 ppm range that account for all imino protons of the α-OH-PdG•dA duplex (Figure 4). Assignment of these signals results from the analysis of a NOESY (220 ms mixing time) spectrum recorded under identical experimental conditions. Each thymine imino proton exhibits characteristically strong NOE peaks with the H2 proton of the counter base adenine across A•T base pairs of the duplex (Figure 4, peaks A–D). Similarly, each guanine imino proton interacts with the hydrogen-bonded and exposed amino protons of their partner cytosine residues across the G•C pairs of the α-OH-PdG•dA duplex (Figure 4, peaks E/E'–H/H'). As in the case of the '100%' D_2O NOESY spectra, the chiral center of α-OH-PdG splits proton signals at the lesion site of the duplex (Figure 4). The spectrum also shows several cross-peaks between adenine H2 and neighboring guanine H1 protons (Figure 4, peaks I, K–N) and between imino protons of adjacent base pairs (Figure 3S, Supplementary Material) indicating extensive base pair stacking throughout the α-OH-PdG•dA duplex.

Several signals appear between 9.75 ppm and 8.27 ppm that belong to the exchangeable protons of the damaged α-OH-PdG•dA mispair. The signals centered at 9.66 ppm and 8.42 ppm display a strong NOE interaction (Figure 4, peak O), indicating a very short distance between these protons and suggesting they belong to the hydrogen bonded and exposed amino protons of A17. In agreement with this assignment, these signals display NOE interactions with the hydrogen bonded and non-hydrogen bonded amino protons of the flanking C5 residue (Figure 4, peaks P/P' and Q/Q', respectively). It is worth noting that these amino protons resonate notably downfield from the value normally observed when they participate in Watson-Crick hydrogen bonds. Their chemical shifts are entirely consistent with the protonation of A17 at the N1 position, that would favor the stabilization of the α-OH-PdG(*syn*)•dA^+(*anti*) base pair by formation of an additional hydrogen bond. In the 1D spectrum of the duplex recorded at 5°C there is a broad proton signal at around 16.0 ppm that accounts for the A^+17(N1H) proton (Figure 4S, Supplementary Material). Due to

its fast T2 relaxation however, the A^+17(N1H) signal lacks interactions in the NOESY spectra recorded under the same experimental conditions, precluding its structural characterization any further. In addition to the A17 interactions, the amino proton of α-OH-PdG exhibit NOE interaction with its vicinal Hα proton in the hydroxypropyl ring of the lesion (Figure 4, peak R). The chemical shift of the exchangeable protons on the α-OH-PdG•dA duplex are also listed in Table 1S (Supplementary Information).

α-OH-PdG•dA duplex structures

Figure 5 presents the *R* and *S* α-OH-PdG•dA duplexes structures, obtained with the A17 residue protonated at N1 during rMD and Figure 5S (Supplementary Material) shows a stereo view of the duplexes. The structures are in excellent agreement with the experimental NMR constraints, exhibiting no inter-proton distance violations >0.5 Å and only minor distortions of the atom covalent geometry (Table 1). The isomeric structures are very similar, revealing an all-atom RMSD of 0.94 Å for the entire duplex, 1.02 Å at the lesion site (central three base pairs) and 0.84 Å for the undamaged eight base pairs at the ends of the duplex (four on each side). The protonation status of A17 has no appreciable effect on the final refined models, since the structures obtained with or without A17 protonation are quite similar and the non-protonated models have slightly smaller RMSD (Figure 6S Supplementary Material).

Both duplexes are regular right-handed helices minimally perturbed by the presence of the α-OH-PdG adduct. The glycosidic torsion angle (χ) of all undamaged residues is in *anti* orientation, with the sugar conformations in the expected C1'-exo/C2'-endo range and regular WC alignments stabilizing the non-damaged base pairs of the duplex. The χ torsion angle of α-OH-PdG is practically identical for both isomers and is within the *syn* range (Table 1), resulting in the Hoogsteen edge of the adduct facing the protonated A17 counter base and the exocyclic 1,N^2-hydroxylpropyl ring positioned in the major groove of the duplex.

Figure 6 displays a magnified structural view of the lesion site, depicting hydrogen bond interactions that stabilize the *syn* conformation of the adduct. Both isomers have a well-formed hydrogen bond between a phosphate oxygen and the remaining amino proton of the adduct. In the case of the *R* duplex, there is an additional hydrogen bond between the same phosphate oxygen and the hydroxyl group of α-OH-PdG. This interaction is missing in the case of the *S* duplex since its (OH)α group points to the 3'-end of the duplex. In addition to these intra-residue interactions, the Hoogsteen edge of the adduct forms hydrogen bonds with A17, its counter base on the complementary strand. In both duplexes, there is a strong hydrogen bond between the imino proton of $A17^+$ and α-OH-PdG(N7) and a second one between A17(N6H) and α-OH-PdG(O6) of less favorable geometry (Table 1, and Figures 6 and 7). The lesion-flanking base pairs adopt regular Watson-Crick alignments, thereby preserving base stacking interactions at the center of the α-OH-PdG•dA duplex (Figure 7). Table 1 lists some statistics of the refinement and hydrogen bond parameters for the α-OH-PdG•dA duplex.

DISCUSSION

NMR spectra

The sequential proton interactions observed in all NOESY spectra collected at 25°C (Figures 2 and 2S, Supplementary Material) in conjunction with the inter strand NOEs detected among exchangeable protons of the duplex (Figure 4) confirms the regular right-handed helical conformation of the α-OH-PdG•dA duplex in solution. The presence of NOE peaks between the C(H5) and its 5'-flanking base proton and the between A(H2) and neighboring

sugar-H1' protons (Figure 2) are additional proof of a regular B-form structure. Furthermore, NOE interactions between sequential imino protons (Figure 3S, Supplementary Material), imino and amino protons, and imino and A(H2) protons of flanking base pairs (Figure 4) are indicative of normal WC base pairing with proper stacking throughout the α-OH-PdG•dA duplex. As in the case of the α-OH-PdG•dC duplex (26), α-OH-PdG maintains the exocyclic ring form when paired with dA, thus preserving chiral center (Cα) of the lesion. The latter causes splitting of NMR signals for residues located either at or near the damaged site with isomer-specific resonances resolved under the experimental conditions (Figures 2–4). Chemical shift differences between corresponding protons of the *R* and *S* duplexes are small (Table 1S, Supplementary Material), indicating that both duplexes adopt a similar conformation in solution. On the other hand, comparison of the α-OH-PdG•dC (26) and α-OH-PdG•dA chemical shifts reveal distinct variations at the lesion containing and the neighboring base pairs, which are characteristic of structural differences. Analysis of NOESY spectra reveals a very strong cross-peak between the H8 and H1' protons of the adduct (Figure 2, peaks X6), indicating a short distance and suggesting a *syn* glycosidic torsion angle. Further evidence for the *syn* conformation of α-OH-PdG are the α-OH-PdG(Hα)-C5(H6) (Figure 2, peak A) and α-OH-PdG(Hγ/γ')-C5(H5) (Figure 3, peaks F and G) NOE peaks, which are close (less than 4.5Å) only with the lesion in *syn* conformation. Significantly, the α-OH-PdG•dC duplex displays identical NOE interactions (26), which suggests that the glycosidic torsion angle of the damaged residue is very similar for both duplexes.

The *syn* glycosidic torsion angle relieves potential steric clashes that would exist across the α-OH-PdG•dA base pair and favors hydrogen bonding with the Hoogsteen edge of the lesion. The 1.23 ppm chemical shift difference between the amino protons of A17 is a strong NMR indication of hydrogen bonding (Figure 4 and Table 1S), a fact subsequently supported by the MD refined three-dimensional structure. Furthermore, the broad 16.0 ppm signal detected at 5°C (Figure 4S, Supplementary Material) in a region normally devoid of proton resonances, suggest formation of an additional hydrogen bond following A17 protonation. The observation that the thermal stability of the duplex is higher in the pH 5.0–6.8 range (unpublished results) provides independent support for the existence of such a hydrogen bond.

Structure of α-OH-PdG•dA duplexes

The presence of the α-OH-PdG•dA mismatch at the center of the duplex induces minor perturbations on the regular right-handed helical structure. Following rotation to a *syn* conformation, the lesion hydroxypropano ring resides in the major groove, where it can be accommodated without causing mayor structural perturbations (Figure 5). As in the case of the α-OH-PdG•dC duplex, adduct chirality is mostly inconsequential since isomeric duplexes have an RMSD of 0.94 Å, and only slightly larger at the three central base pair segment. In both isomers, a well-formed hydrogen bond between the amino proton (N2H) and the phosphate group of α-OH-PdG stabilizes the *syn* conformation of the damaged residue, with a second hydrogen bond between α-OH-PdG(OHα) and the same phosphate oxygen that is only present in the *R* duplex (Figure 6). While direct evidence for these hydrogen bonds is not observed in the NMR spectra, the downfield value of the α-OH-PdG(N2H) proton at 8.71 ppm and 8.53 ppm for the *R* and *S* isomers (Figure 4 and Table 1S) supports its involvement in hydrogen bonding.

When α-OH-PdG is in the *syn* conformation, two hydrogen bonds form across the α-OH-PdG•dA mismatch involving the protonated A17(N1H) and A17(N6H) as donors and the α-OH-PdG(N7) and α-OH-PdG(O6) as respective acceptors (Figure 7). These hydrogen bonds parallel those observed across the α-OH-PdG•dC^+ pair (26) yet are stronger and form more readily, occurring in all of the refined structures. Duplex models obtained by running rMD

with a non-protonated dA17 residue have almost identical donor-acceptor distances (data not shown), which suggests that upon α-OH-PdG adopting a *syn* conformation, the subsequent formation of hydrogen bonds requires minimal structural adjustment. Furthermore, the C1'-C1' distance across the α-OH-PdG•dA pair is similar, or just slightly larger, than that of the flanking C•G base pairs. In summary, these properties may explain why the α-OH-PdG•dA mismatch-containing duplex is more stable than its α-OH-PdG•dC counterpart (Minetti et al., companion manuscript, (41)).

Biological implications

It has been established that the α-OH-PdG adduct of acrolein extensively blocks DNA replication in human cells, a finding consistent with the significant α-OH-PdG-induced reduction in duplex dissociation free energy and melting cooperativity (Minetti et al., companion manuscript, (41)). When bypassed by translesion synthesis (TLS) polymerases, α-OH-PdG primarily codes for dC incorporation along with A and T, thereby resulting in G → T and G → A base substitution mutations (24). Primer extension studies using recombinant TLS polymerases reveals that whereas Polη and Polκ participate in error prone replication of the lesion, Rev1 and Polι favor dC insertion opposite the lesion with the latter incorporating dA and T at a lower frequency (37). The X-ray structure of a ternary Rev1-dCTP-damaged DNA complex reveals that the PdG residue (an analog of α-OH-PdG that lacks the hydroxyl group) is extruded into a small pocket with sufficient room to accommodate the hydroxyl group of both α-OH-PdG isomers. Concurrently, the incoming dCTP forms two hydrogen bonds with an active site arginine residue, thereby explaining the Rev1 preference for dCTP incorporation. Importantly, the extruded PdG residue adopts an *anti* conformation suggesting that Rev1 needs to break the hydrogen bonds that favor an α-OH-PdG *syn* conformation prior to attaining such a structure (38). Polι, on the other hand, incorporates dNTP opposite a damaged template residue that adopts the *syn* conformation (39,40). The structures of the α-OH-PdG•dC (26) and α-OH-PdG•dA duplexes have identified specific molecular interactions that 'lock' α-OH-PdG in a *syn* configuration, suggesting a Polι advantage for catalyzing the incorporation of either dCTP or dATP during lesion replication since it encounters a favorable template conformation.

Supplementary Material

Refer to Web version on PubMed Central for supplementary material.

Abbreviations

NMR	nuclear magnetic resonance
EDTA	disodium ethylenediamine tetracetate
TSP	sodium 3-trimethylsilyl-propionate-2,2,3,3,-d_4
NOESY	nuclear Overhauser effect spectroscopy
COSY	correlation spectroscopy
DQF-COSY	double quantum filtered correlation spectroscopy
TOCSY	total correlation spectroscopy
NOE	nuclear Overhauser effect
rMD	restrained Molecular Dynamics
hb	hydrogen-bonded

nhb	non-hydrogen-bonded
WC	Watson-Crick
rsmd	root mean square deviation
TLS	trans lesion synthesis

Acknowledgments

Research supported by NIH Grant CA47995.

REFERENCES

1. Izard C, Libermann C. Mutat. Res. 1978; 47:115–138. [PubMed: 415230]
2. Roemer E, Stabbert R, Rustemeier K, Veltel DJ, Meisgen TJ, Reininghaus W, Carchman RA, Gaworski CL, Podraza KF. Toxicology. 2004; 195:31–52. [PubMed: 14698566]
3. Zhang S, Villalta PW, Wang M, Hecht SS. Chem Res Toxicol. 2007; 20:565–571. [PubMed: 17385896]
4. Esterbauer H, Schaur RJ, Zoller H. Free Rad Biol Med. 1991; 11:81–128. [PubMed: 1937131]
5. Wu H-Y, Lin Y-L. Anal Chem. 1995; 76:1603–1612.
6. Chung FL, Nath RG, Nagao M, Nishikawa A, Zhou GD, Randerath K. Mutat Res. 1999; 242:71–81. [PubMed: 10064851]
7. Lee Y, Sayre LM. J Biol Chem. 1998; 273:19490–19494. [PubMed: 9677370]
8. Alarcon RA. Cancer Treat Rep. 1976; 60:327–335. [PubMed: 1277208]
9. McDiarmid MA, Iype PT, Kolodner K, Jacobson-Kram D, Strickland PT. Mutat. Res. 1991; 248:93–99. [PubMed: 2030715]
10. Galliani G, Pantarotto C. Tetrahedron Lett. 1983; 24:4491–4492.
11. Chung FL, Young R, Hecht SS. Cancer Res. 1984; 44:990–995. [PubMed: 6318992]
12. Esterbauer H, Schaur R, Zollner H. Free Radical Biol Med. 1991; 11:81–128. [PubMed: 1937131]
13. Uchida K, Kanematsu M, Sakai K, Matsuda T, Hattori N, Mizuno Y, Suzuki D, Miyata T, Noguchi N, Niki E, Osawa T. Proc Natl Acad Sci USA. 1998; 95:4882–4887. [PubMed: 9560197]
14. Marnett LJ, Hurd HK, Hollstein MC, Levin DE, Esterbauer H, Ames BN. Mutat Res. 1985; 148:25–34. [PubMed: 3881660]
15. Curren RD, Yang LL, Conklin PM, Grafstrom RC, Harris CC. Mutat Res. 1988; 209:17–22. [PubMed: 3173398]
16. Smith RA, Cohen SM, Lawson TA. Carcinogenesis. 1990; 11:497–498. [PubMed: 2311195]
17. Kawanishi M, Matsuda T, Nakayama A, Takebe H, Matsui S, Yagi T. Mutat Res. 1998; 417:63–75.
18. Khullar S, Varaprasad CV, Johnson FJ. Med Chem. 1999; 42:947–950.
19. Nechev LV, Harris CM, Harris TM. Chem Res Toxicol. 2000; 13:421–429. [PubMed: 10813660]
20. Huang Y, Torres MC, Iden CR, Johnson F. Bioorg Chem. 2003; 31:136–148. [PubMed: 12729571]
21. Yang I-Y, Hossain M, Miller H, Khullar S, Johnson F, Grollman A, Moriya M. J Biol Chem. 2001; 276:9071–9076. [PubMed: 11124950]
22. Vander Veen LA, Hashim MF, Nechev LV, Harris TM, Harris CM, Marnett LJ. J Biol Chem. 2001; 276:9066–9070. [PubMed: 11106660]
23. Yang I-Y, Johnson F, Grollman AP, Moriya M. Chem Res Toxicol. 2002; 15:160–164. [PubMed: 11849041]
24. Yang I-Y, Chan G, Miller H, Huang Y, Torres MC, Johnson F, Moriya M. Biochemistry. 2002; 41:13826–13832. [PubMed: 12427046]
25. de los Santos C, Zaliznyak T, Johnson F. J Biol Chem. 2001; 276:9077–9082. [PubMed: 11054428]

26. Zaliznyak T, Bonala R, Attaluri S, Johnson F, de los Santos C. Nucleic Acids Res. 2009; 37:2153–2163. [PubMed: 19223332]
27. States DJ, Habekorn RA, Ruben DJ. J Mag Res. 1982; 48:286–292.
28. Plateau P, Gueron MJ. Am. Chem. Soc. 1982; 104:7310–7311.
29. Brünger, A. XPLOR Version 3.1 A system for X-Ray Crystallography and NMR. New Haven, CT: Yale Univ. Press; 1993.
30. Brooks BR, Buccoleri RE, Olafson BD, States DJ, Swaminathan S, Karplus M. J Comput Chem. 1983; 4:187–217.
31. Friedman RA, Honig B. Biopolymers. 1992; 32:145–159. [PubMed: 1637989]
32. Yip P, Case DA. J Magn Reson. 1989; 83:643–648.
33. Lavery R, Sklenar H. J Biomol Struct Dyn. 1988; 6:655–667. [PubMed: 2619933]
34. Pettersen EF, Goddard TD, Huang CC, Couch GS, Greenblatt DM, Meng EC, Ferrin TE. J Comput Chem. 2004; 25:1605–1612. [PubMed: 15264254]
35. van de Ven FJM, Hilbers CW. J Biochem. 1988; 178:1–38.
36. de los Santos, C. Comprehensive Natural Products Chemistry. Vol. Vol. 7. Oxford: Elsevier Science Ltd; 1999. Probing DNA Structure by NMR Spectroscopy.
37. Sanchez AM, Minko IG, Kurtz AJ, Kanuri M, Moriya M, Lloyd R;S. Chem Res Toxicol. 2003; 16:1019–1028. [PubMed: 12924930]
38. Nair DT, Johnson RE, Prakash L, Prakash S, Aggarwal AK. Structure. 2008; 16:239–245. [PubMed: 18275815]
39. Nair DT, Johnson RE, Prakash S, Prakash L, Aggarwal AK. Nature. 2004; 430:377–380. [PubMed: 15254543]
40. Prakash S, Johnson RE, Prakash L. Eukaryotic translesion synthesis DNA polymerases: Specificity of Structure and Function. Annu. Rev. Biochem. 2005; 74:317–353. [PubMed: 15952890]
41. Minetti CASA, Remeta DP, Breslauer K. Biopolymers. (companion manuscript).

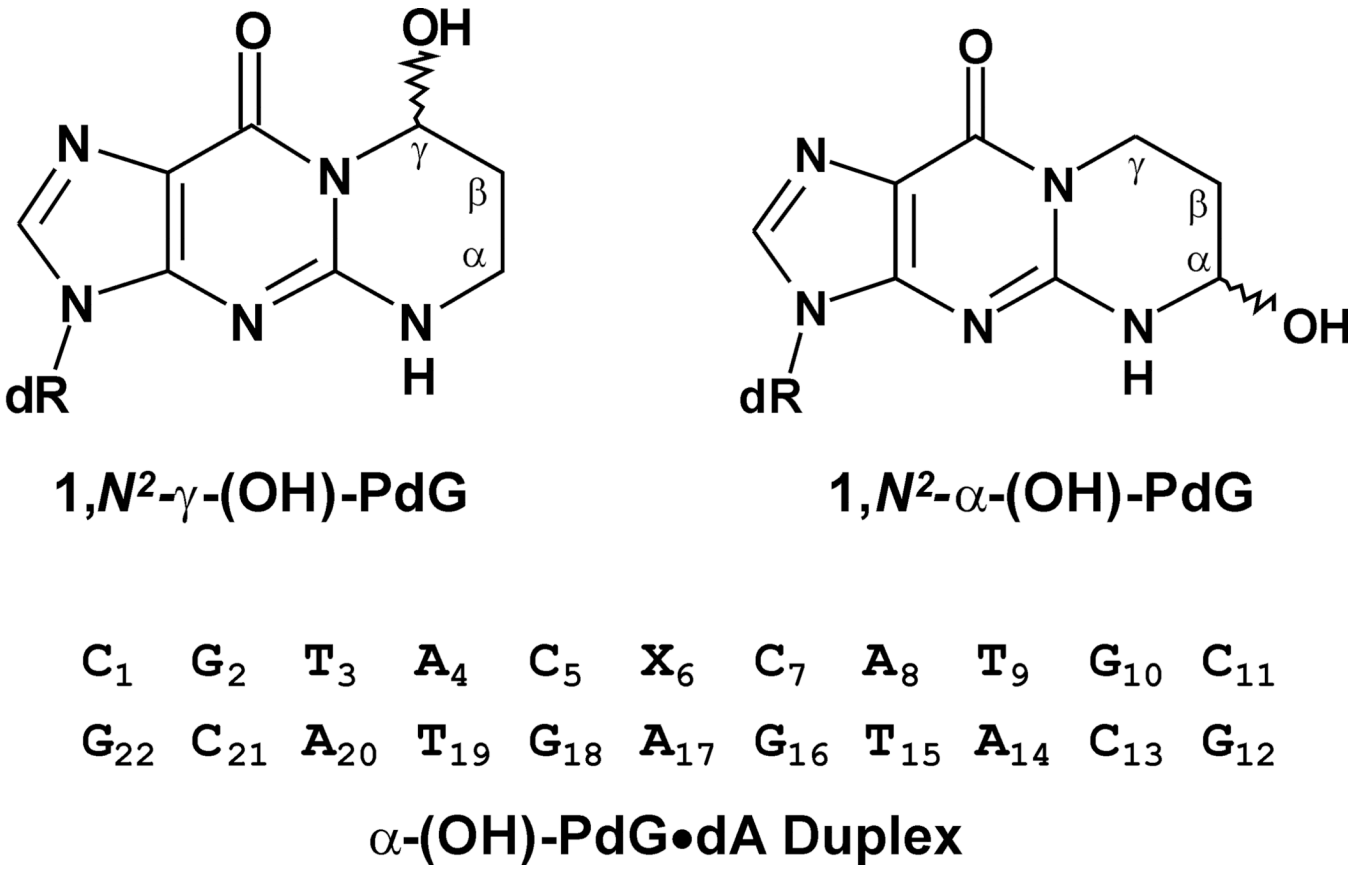

Figure 1.
Chemical structure of acrolein adducts and sequence composition of the α-OH-PdG•dA duplex.

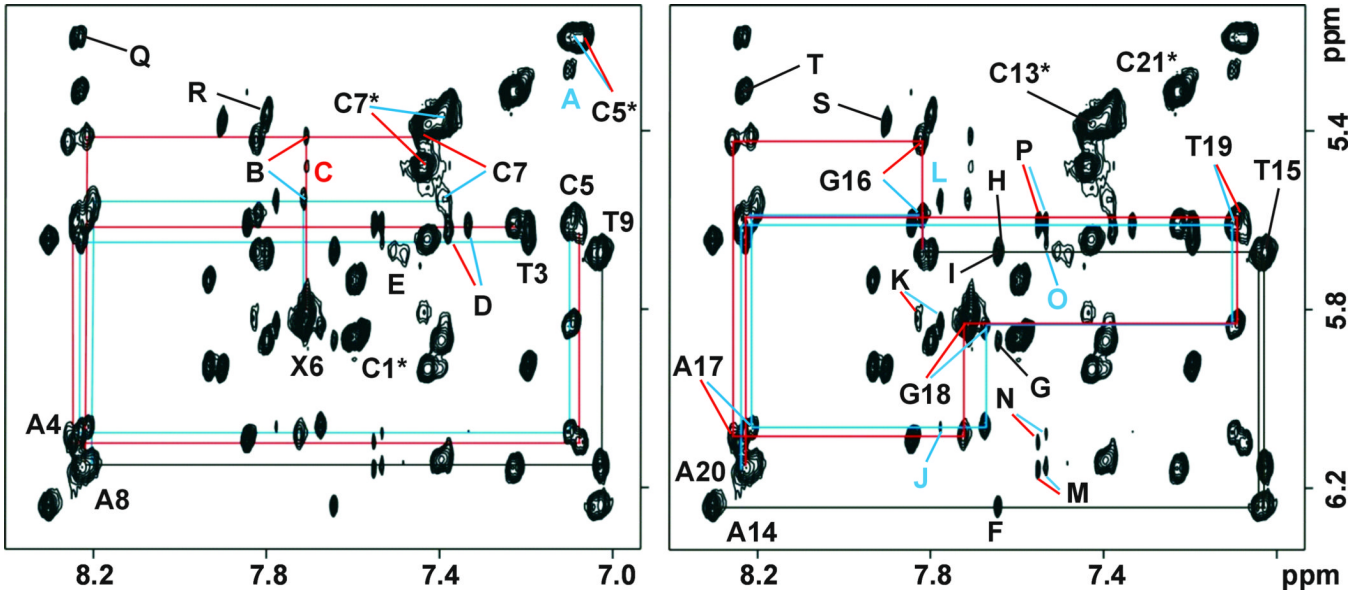

Figure 2.

Expanded region of a 600 MHz NOESY (300 ms mixing time) spectrum recorded at 25°C with the sample dissolved in '100%' D_2O phosphate buffer, pH 6.6, containing 50 mM NaCl and 1 mM EDTA. The figure displays the 'finger print' region of the spectrum showing the sequential interactions between base (6.94–8.40 ppm) and the sugar H1' (5.12–6.34 ppm) protons, from T3 through T9 on the damaged strand (left) and from A14 through A20 on unmodified strand (right). Residue labels indentify intraresidue base-H1' NOEs, with X6 being that of α-OH-PdG, and asterisks indicate cytosine H6-H5 interactions. Blue and red colors differentiate resolved NOE peaks originated from the *S* and *R* enantiomers, respectively. Other labels are assigned as follows: A, X6(Hα)-C5(H6); B, X6(H8)-C7(H1'); C, X6(H8)-C7(H5); D, A4(H2)-C5(H1'); E, A8(H2)-T9(H1'); F, A14(H2)-A14(H1'); G, A14(H2)-G10(H1'); H, A14(H2)-T9(H1'); I, A14(H2)-T15(H1'); J, A17(H2)-A17(H1'); K, A17(H2)-G18(H1'); L, A17(H2)-C7(H1'); M, A20(H2)-A20(H1'); N, A20(H2)-A4(H1'); O, A20(H2)-T3(H1'); P, A20(H2)-C21(H1'); Q, A4(H8)-C5(H5); R, G10(H8)-C11(H5); S, G12(H8)-C13(H5); T, A20(H8)-C21(H5).

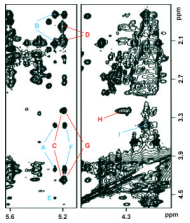

Figure 3.

Expanded contour plots of regions of a 600 MHz NOESY (300 ms mixing time) spectrum recorded at 25°C with the sample dissolved in '100%' D_2O phosphate buffer, pH 6.6, containing 50 mM NaCl and 1 mM EDTA, depicting NOE interactions of the exocyclic α-OH-PdG protons. Blue and red labels differentiate peaks originated from the *S* or *R* enantiomer, respectively. Labels are assigned as follows: A, X6(Hα)-X6(Hγ/γ'); B, X6(Hα)-X6(Hβ/β'); C, X6(Hα)-X6(Hγ/γ'); D, X6(Hα)-X6(Hβ/β'); E, C5(H3')-X6(Hα); F, C5(H5)-X6(Hγ/γ'); G, C5(H5)-X6(Hγ/γ'); H, X6(Hγ)-X6(Hγ'); I, X6(Hγ)-X6(Hγ'). The geminal β and γ protons of α-OH-PdG were not stereo specifically assigned.

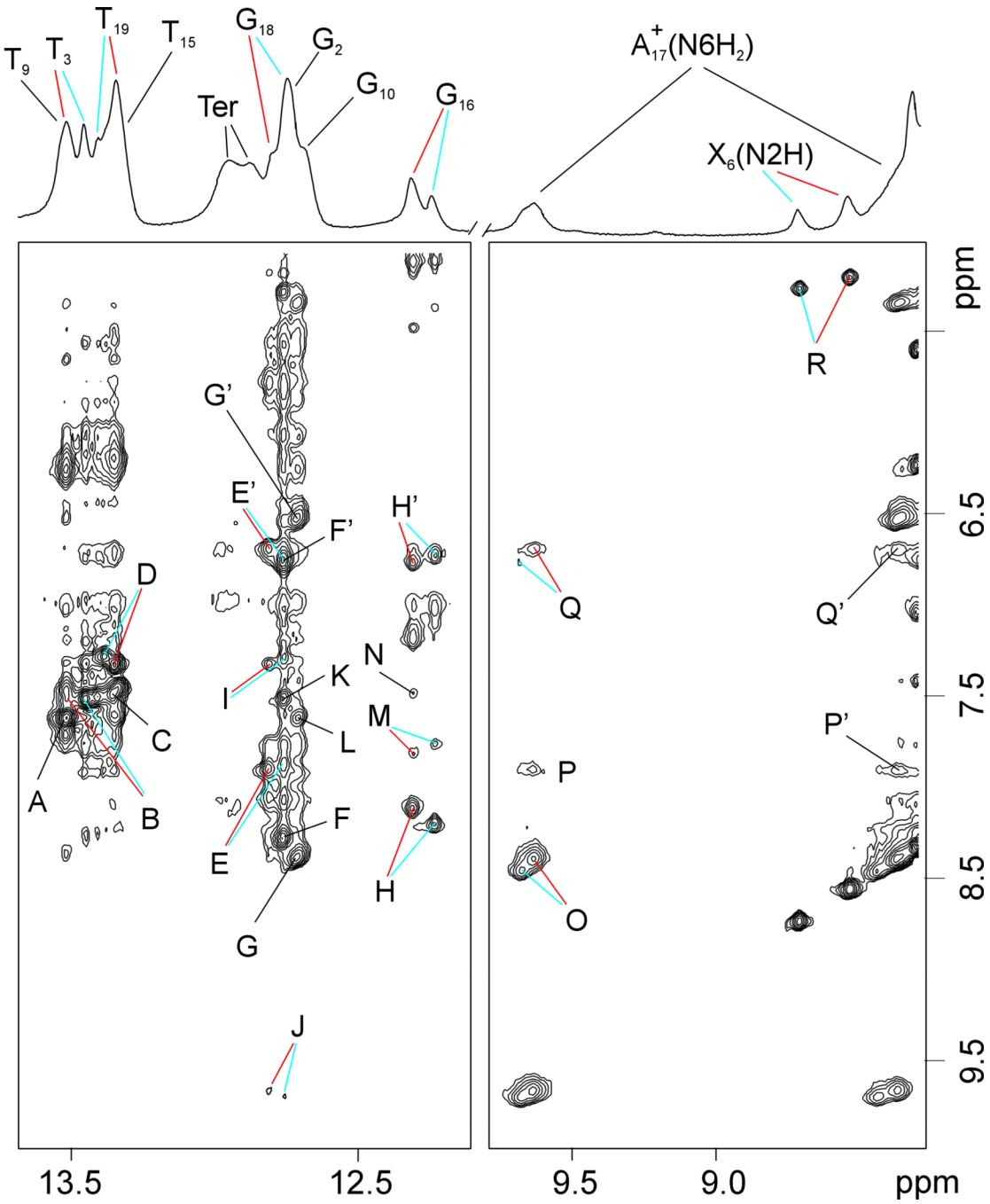

Figure 4.

Expanded regions of a 600 MHz NOESY (220 ms mixing time) spectrum recorded at 5°C with the α-OH-PdG•dA duplex dissolved in 10% D_2O phosphate buffer, pH 6.6, containing 10 mM phosphate, 50 mM NaCl and 1 mM EDTA, and a 1D trace shown on top. The figure depicts NOE interactions involving the exchangeable protons. Blue and red labels differentiate peaks originated from the *S* and *R* enantiomers, respectively. Labeled peaks are assigned as follows: A, T9(N3H)-A14(H2); B, T3(N3H)-A20(H2); C, T15(N3H)-A8(H2); D, T19(N3H)-A4(H2); E, G18(N1H)-C5(N4H)$_{hb}$; E', G18(N1H)-C5(N4H)$_{nhb}$; F, G2(N1H)-C21(N4H)$_{hb}$; F', G2(N1H)-C21(N4H)$_{nhb}$; G, G10(N1H)-C13(N4H)$_{hb}$; G', G10(N1H)-C13(N4H)$_{nhb}$; H, G16(N1H)-C7(N4H)$_{hb}$; H', G16(N1H)-C7(N4H)$_{nhb}$; I, G18(N1H)-

A4(H2); J, G18(N1H)-A17(N6H)$_{hb}$; K, G2(N1H)-A20(H2); L, G10(N1H)-A14(H2); M, G16(N1H)-A17(H2); N, G18(N1H)-A8(H2); O, A17(N4H)$_{hb}$-A17(N4H)$_{nhb}$; P, A17(N4H)$_{hb}$-C5(N4H)$_{hb}$; P', A17(N4H)$_{nhb}$-C5(N4H)$_{hb}$; Q, A17(N4H)$_{hb}$-C5(N4H)$_{nhb}$; Q', A17(N4H)$_{nhb}$-C5(N4H)$_{nhb}$; R, X6(N2H)-X6(Hα). Hb and nhb stand for hydrogen bonded and non-hydrogen-bonded.

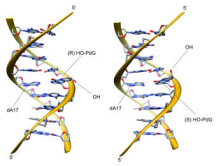

Figure 5.
Stick-ribbon representation of isomeric α-OH-PdG•dA duplex structures shown with the major groove prominent. Atoms are colored by type with the backbone in green.

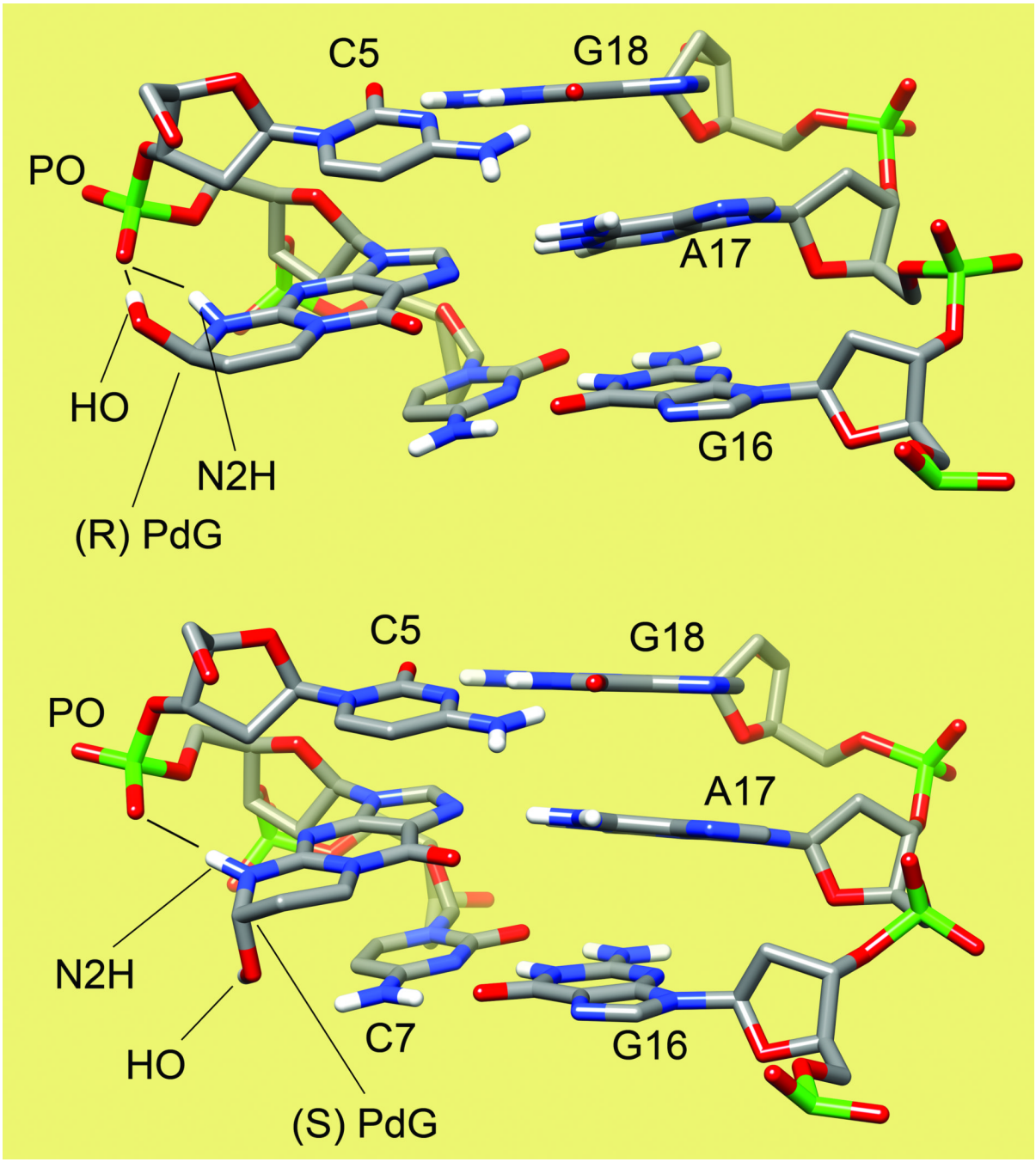

Figure 6.
Close up view of the central three base pair fragment depicting hydrogen bond interactions that stabilize the *syn* conformation of α-OH-PdG. For clarity, the chain orientation in this figure is different from that in Figure 5.

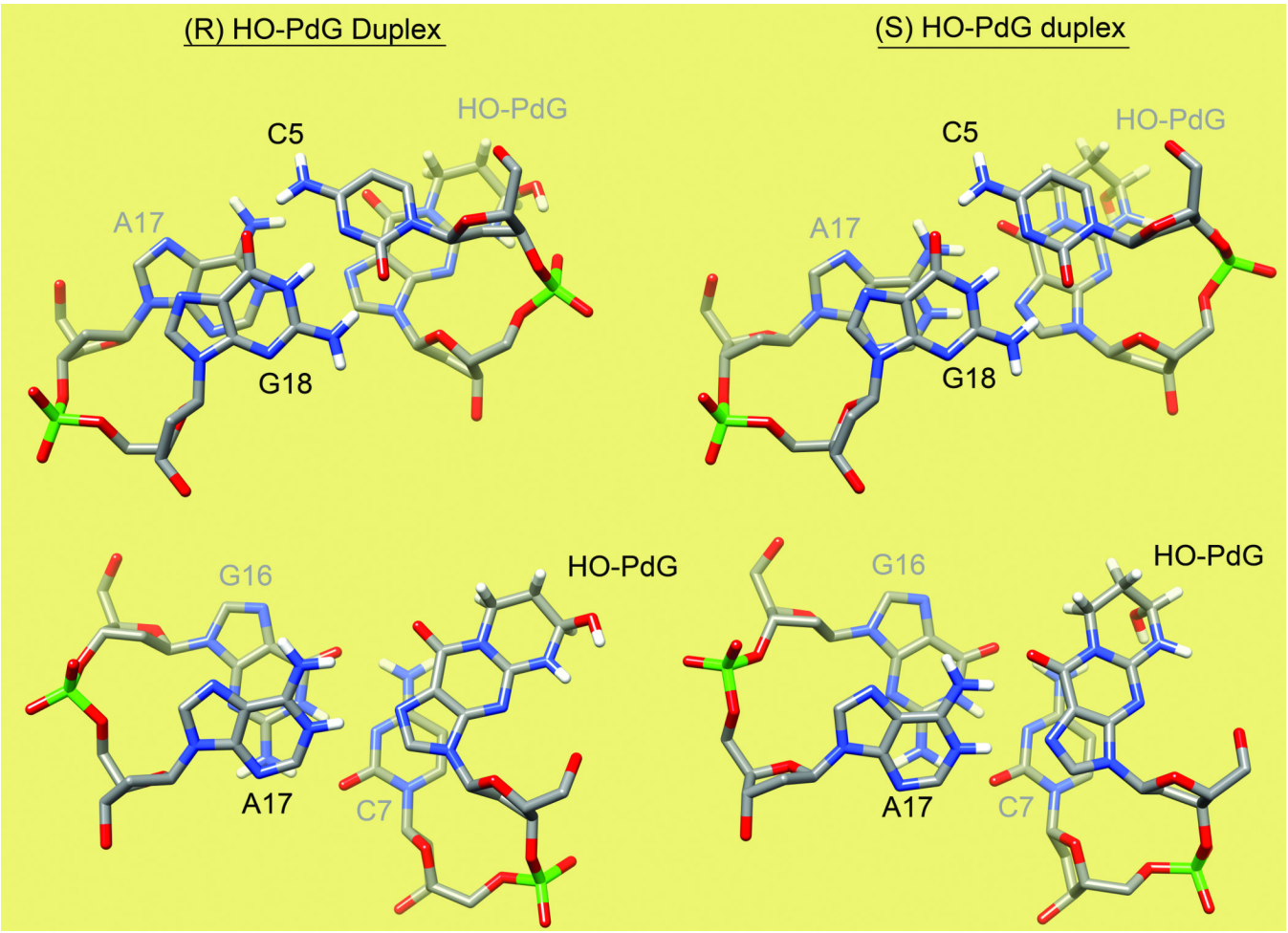

Figure 7.
Hydrogen bonds and staking interactions at the lesion site of the α-OH-PdG•dA duplex.

Table 1

Statistics of the refinement and structural parameters of α-OH-PdG•dA duplexes[a]

	***R*-isomer**	***S*-isomer**
NOE Distance and Covalent Geometry Violations		
RMSD NOE-Violations (Å)	0.046	0.045
Number of Distance Violations (<0.1Å)[b]	4 (3)	7 (2)
RMSD Bond Lengths (Å)	0.006	0.005
RMSD Bond Angles (°)	2.28	2.22
Van der Waals Energy (Kcal/mol)	−343	−348
Lesion Site Hydrogen Bonds		
α-OH-PdG (N2H-O2P) distance (Å) & (N2-H2-O2P) angle (°)	2.11 / 162	2.33 / 169
α-OH-PdG (OHα-O2P) distance (Å) & (Oα-Hα-O2P) angle (°)	2.16 / 172	4.65 / 102
α-OH-PdG(O6)-A17$^+$(N6H) distance (Å) & (O6-N6H-N4) angle (°)	3.65 / 150	2.20 / 139
α-OH-PdG(N7)-A17$^+$(N1H) distance (Å) & (N7-N1H-N1) angle (°)	2.22 / 171	2.26 / 172

[a] Averaged values computed from the 25 final structures refined with protonated lesion site dA.

[b] In parenthesis are NOE violations at the central three base pair segment. Chi torsion angles of the *R* and *S* α-OH-PdG were 59° and 60°, respectively.